Organic & Supramolecular Chemistry

The Importance of Polymorphism Dependent Aggregation Induced Enhanced Emission of the Acrylonitrile Derivative: Helical *J* Type and Antiparallel *H* Type Stacking Modes

Gül Yakalı,*[a] Mustafa B. Çoban,[b] Furkan Özen,[c] Leyla B. Özen,[c] Bayram Gündüz,[d] and Günseli Turgut Cin[e]

In this study to analyze the structure-property relationship of synthesized π-conjugated acrylonitrile derivative in terms of polymorphism dependent emission and conformational polymorphism, single crystal x-ray diffraction method, photophysical and theoretical studies were performed. The fluorescent molecule with two polymorphic structure were presented to demonstrate the effect of the molecular conformation and stacking type on the polymorphism dependent emission in aggregate state. According to results of crystallography and photophysical studies, both form of the molecule displayed aggregation induced enhanced emission (AIEE) property in the solid phase due to the restricted intramolecular rotation (RIR) and favourable stacking interactions including the antiparallel *H type, J type* stacking modes and intramolecular charge transfer (ICT) process. As a result, *J type* and antiparallel *H type* stacking mode with the restricted intramolecular rotation make the crystals higly emissive in solid phase. We believe that, studied two polymorphs will be best candidates for the π-conjugated acrylonitrile derivatives in the optoelectronic field. Moreover, this study will provide an overview of the importance of conformational polymorphism, stacking type on fluorescence properties of the polymorphic structures and propose new ways for targeted polymorphic molecular design strategies in acrylonitrile derivatives.

Introduction

Examination of the molecular structure to determine the properties of the organic optoelectronic materials which is often obtained by using π-conjugated molecules plays an important role in the design of new materials with desired properties.[1–6] The design and synthesis of them have great attention due to having possible applications in organic electroluminescent devices organic light-emitting diodes, (OLEDs), organic thin-film transistors (OTFTs), light-emitting cells (LEC) and organic photovoltaic diodes (OPVDs).[7–10] Interest in organic π-conjugated molecules for optoelectronic applications has increased efforts to figure out the relationship between the charge transport properties and the crystal structure of these molecules therefore structure-property relationship of them.[11–14] The charge transport properties in small organic molecules is strongly depends on the intermolecular stacking interactions which are defined by π-orbital overlap between the ring systems. Therefore, even the smallest change in molecular packing mode of the molecules affects their π stacking interactions especially stacking type (*H type, J type, T type and herringbone*) or π-orbital overlap which can cause changes in charge transport properties of the molecules.[15–17] One of the ways to analyze the effect of different packing modes on optoelectronic charge transport related to photoluminesans behavior of the molecules or device performance is to create polymorphic crystal structures that they enable a unusual opportunity to carried out the structure property relationship.[18–21] Therefore, different polymorphs often have distinct physical properties such as the crystal habits, melting point, solubility, electronic, optical and mechanical properties. The most general definition of polymorphism process is to discovered the multiple crystalline packing states of the same molecule under the different conditions including growth process or subsequent treatment by variations in different physical parameters such as temperature, solvent effects, grinding and sublimation and it has significant results in material science.[22–24] The formation of

[a] *Dr. G. Yakalı*
Department of Engineering Sciences,
Faculty of Engineering,
Izmir Katip Celebi University,
Cigli, 35620 Izmir, Turkey
E-mail: gul.yakali@ikcu.edu.tr
[b] *Dr. M. B. Çoban*
The Center of Science and Technology Application and Research,
Balıkesir University,
Bigadiç, 10145
Balıkesir, Turkey
[c] *Dr. F. Özen, Ph. D. L. B. Özen*
Department of Mathematics and Science,
Faculty of Education,
Akdeniz University,
Konyaaltı, 07058
Antalya, Turkey
[d] *Dr. B. Gündüz*
Department of Opticians,
Malatya Turgut Ozal University,
44210 Malatya, Turkey
[e] *Prof. G. T. Cin*
Department of Chemistry, Faculty of Science, Akdeniz University,
Konyaaltı, 07058 Antalya, Turkey

Supporting information for this article is available on the WWW under https://doi.org/10.1002/slct.202102018

© 2021 Wiley-VCH GmbH

different crystal structure of the same molecule with the grinding and sublimation process recognized by differences in the colour and shape of crystals that this situation is termed the conformational polymorphism occasionally contains existence of more than one conformer in the asymmetric unit of same crystal structure (Z).[25,26] However, when the difference between the polymorphic structure arise from various crystal packing arrangements, it is termed as packing polymorphism.[27] The both polymorphism type (conformational and packing polymorphism) could be seen at the same time as in our study. Polymorphism provides an excellent platform for examining the fundamental relationship between photoluminesans structure-property relationship therefore optoelectronic device performance because of the undisputed crystallographic data and obtainable emission characteristics.[28–34] Our work in this paper provide an overview of the conformational and packing poylmorphism in organic small molecules to investigate the structure-property relationship based on the photoluminesans behavior of the polymorphs in the optoelectronic field.

The most popular method to reveal the structure-property relationship of polymorphic structures is the single crystal x-ray diffraction method (SCXRD). SCXRD has the great advantage of providing detailed 3D structural information on the molecular geometry and controlling the packing modes of the molecules in the crystal. In addition, it provide detailed information about structural role of solvent molecules through the noncovalent interactions such as, intra and intermolecular hydrogen bonding, stacking interactions, C-halogen interactions and short interactions with the smaller distance than van der waals radius between the atoms in the molecule. The polymorphic existence of the studied molecule may depend on noncovalent interactions including intra and intermolecular interactions which are affected by crystallization conditions.[35–37] Therefore, understanding of noncovalent interactions in the polymorphic crystal structures has an important place to analyze structural differences and packing modes between them and their charge transport and photoluminesans behavior in solid phase.[38–41] The performance of organic molecule based devices strongly is related to the molecular-assembly structures which are created by interactions of whole molecule in the aggeragate state rather than by individual molecule. It is necessary to elucidate the relationship between molecular packing characteristics formed by noncovalent interactions and optoelectronic properties to meet demands about the new molecular organic functional materials.[42–45]

The packing modes of the conjugated organic small molecules can be created by stacking interactions and short interactions between the atoms in the molecule, coulomb interactions, and van-der-Waals forces.[46,47] Especially, the packing modes formed by intermolecular stacking interactions play a crucial role in the charge transport of the molecules therefore photoluminescent structure-property relationship.[48–50] Five stacking geometries are observed between the two aromatic rings as cofacial (face to face or *H stacking type*), slipped stacking mode (displaced or *J stacking type*), herringbone (edge to face), helical stacking type and *T type* stacking which are seen in the form of the parallel or antiparallel depending on the 3D molecular geometries of them. These stacking types are determined by the calculation method developed by Curtis et all from the single crystal x-ray data and depend on the value of perpendicular distance (d), slippage angle (, pitch and roll angles (P and R, respectively) and pitch and roll distance (d_P and d_R, respectively) between the adjacent rings.[51] According to reported results, the herringbone and slipped stacking modes enhance the charge transport between the adjacent molecules that it result in high mobilities and high photoluminescence intensity.[52,53] Although face to face stacking interactions is formed through more overlap between the rings which is benefical for the charge transfor process of PL behavior, parallel *H stacking type* has a detrimental effect on the device performance of the molecule while antiparallel *H type stacking* mode provide strong emision intensity in the photoluminescence or charge transfer mobility due to both electrostatic potentials on the lateral periphery of the molecules including donor and acceptor groups.

Besides the intermolecular interactions, since the intramolecular stackings, nonclassical hydrogen bonds, short interactions, C-halogen$\cdots\pi$ interaction contribute to molecular rigidity which lead to Restricted Intramolecular Rotation (RIR) process, they have an important place in the analysis of luminescent structure property relationship of the small organic molecules.[54,55] Restricted intramolecular rotation process contains restriction of intramolecular rotations and intramolecular vibrations which are beneficial for the molecule to exhibit very strong luminescence behavior in solid phase. It is worth mentioning that although most -conjugated organic molecules have strong emission in solution phase but in the solid state because of aggregation induced quenching (AIQ), some molecules of same type are nonemissive in solution but highly emissive in solid phase which is termed aggregation induced emission (AIE) and can be attributed to restricted intramolecular rotation.[56,57] To avoid undesirable effect of the AIQ, AIE molecules have attracted increasing attention in recent years. Restricted intramolecular motion constrains the intramolecular rotation of adjacent molecules in solid phase and enable the structural rigidification of molecules which prevents radiationless channels, directing relaxation of excitons through radiative channels and therefore it makes the molecule higly emissive in aggregate state or solid phase. These intramolecular rotations or vibrations in solution cause to radiationless situation in the excited state and result in nonemissive or weak emissive of the molecule in solution. In this study, polymorphism dependent enhanced emission in molecular aggregates based on aggregation induced enhanced emission was investigated in solid phase due to different molecular confomations and packing strucructures of the polymorphic molecules.[58–60]

Here in, we have designed and synthesized a class (E)-2-(3-chlorophenyl)-3-(4-methoxyphenyl)acrylonitrile molecule. This molecule is a class of D-π-A fluorescent compounds where electron acceptors and electron donors were incorporated into the terminal side of the molecule that this method is widely used in the optoelectronic field. The synthesized molecule

© 2021 Wiley-VCH GmbH

demonstrated different two conformation and packing arrangements in the their crystal structures due to the solvent induced polymorphism and free rotation possible around the C–C bonds nearly in the middle of the molecules that this situation resulted in different noncovalent intra and intermolecular interactions. Therefore the conformational polymorphism which have significant effect on the photoluminescence behavior of the molecule in solution and solid phase was observed in the present study. It is shown that these molecules showed polymorphism dependent fluorescence based on aggregation induced enhanced emission which was cerated through restricted intramolecular rotation process (RIR) by using the data of the single crystal x-ray structure and photophysical studies. Different fluorescence emission of the two polymorphic molecules are ascribed to the different π-π stackings between adjacent rings and their conformations. In addition, beside the photophysical and single crystal x-ray crystallographic studies to further obtain molecular characterization of two polymorps, spectroscopic studies (FTIR, ^{1}H-NMR, ^{13}C-NMR and Raman Spectroscopy), Cyclic Voltogram measurements, Termogravimetric Analysis (TGA) were investigated. We hope that, this work provide a practical way to analyze and interpret the luminescent structure-property relationships in polymorphic molecules and polymorphism dependent aggregation induced emission process. Moreover, the obtained results provide in the design of luminescent polymorphs which can enhance significantly contribution to the optoelectronic field.

Result and Discussion

Crystallographic Results

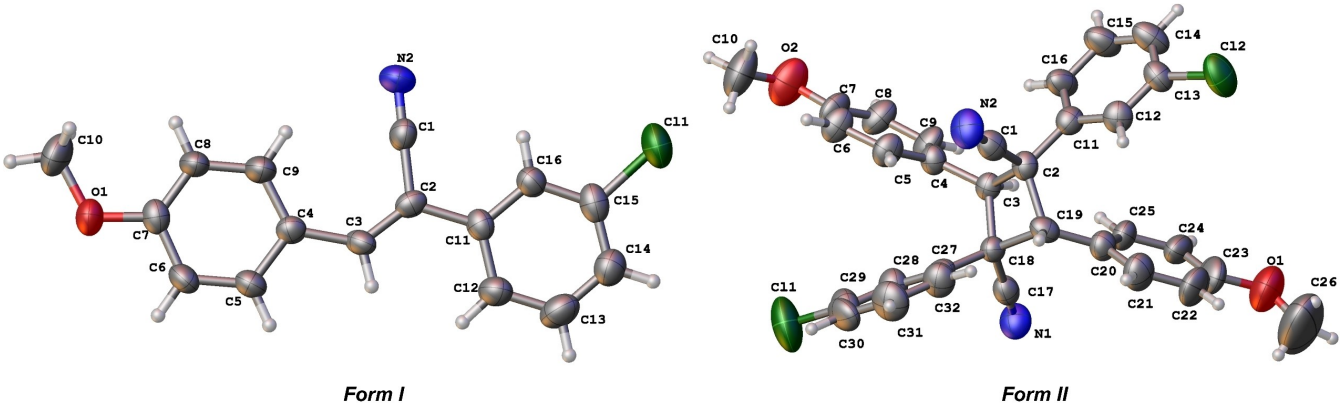
High quality single crystals were used to perform X-ray single-crystal structure analysis. (E)-2-(3-chlorophenyl)-3-(4-methoxyphenyl)acrylonitrile (**1**) molecule has two polymorphisms of *form I and form II* which demonstrate different aggregate states as antiparallel *H type* and *J type*, respectively. The single-crystal X-ray structure of the studied molecule showed that the compound is composed of chlorophenyl (acceptor side) and methoxyphenyl (donor site) rings at terminal region of the molecule which are connected to cyano grup (C) located at the nearly molecule center. The crystallographic data and ortep viewing for both forms of the molecule are given in Table S2 and Figure 1, respectively. All the geometrical parameters of both forms are good aggreement with similar reported structures.[61–63] The differences between the polymorphic forms can be seen from the cell parameters that the crystal structures of the *form I* and *II* are determined by the space group *Cc* (Z = 4) with one of the independent molecules in the asymmetric unit and *P21/c* (Z = 2) with the two independent molecules in the asymmetric unit, respectively. According to Table S1, the cell volume of *form I* is larger than *form II* under the premise that there exist the different number molecules in two different unit cells.

Description of Form I

The single crystal structure of the polymorphic *form I* obtained in acetonitrile is perfectly planar with angles of 1.9 (3) ° between the methoxyphenyl (C4/C9) and chlorophenyl rings (C11/C16). In addition, methoxyphenyl and chlorophenyl rings make the angle of 1.2(2) and 2.9(2) with the molecule plane, respectively. The value of the dihedral angle of C4–C3–C2–C11 is 178.93 (2) which states the π-conjugated part of the molecule is seen to be highly planar.

Description of Form II

The single crystal structure of polymorphic *form II* obtained in ethanol shows two identical independent molecules in asymmetric unit. These two molecules are connect to each other through C2···C19 and C3···C18 short interactions. Unlike *Form I*, this polymorphic structure has higly twisted conformation with the dihedral angle of 57.5 (4) between the methoxyphenyl (C4/C9) and chlorophenyl (C11/C16) rings. In addition, since the molecule tends to rotate around the C–C bonds (C3–C4, C2–C11, C27–C18, C19–C20) diheral angle between the C27/C32 and C20/C25 rings is 41.2(4). All rings in the *form II* are not parallel to molecule plane depending on the avarege dihedral



Form I *Form II*

Figure 1. Single crystal x-ray diffraction ORTEP view of the polymorhic structures with the 50 % probability.

© 2021 Wiley-VCH GmbH

angle of 60. The value of torsion angle of C27–C18–C19–C20, C4–C3–C2–C11 are 137.32 and −89.44, respectively that these result verify existing of nonplanar π-conjugated part of the molecule. The cyano groups on each independent molecule are directed at a different angle which are 178.413 and 177.99 for the up and down molecules, respectively. These large difference in molecular conformation with respect to the *form I* arises from different crystallization condition which depends on solvent and it results in different supramolecular structure and packing modes. Ethanol solvent demonstrated the important role in the crystallisation process of the main molecule. At the molecular level, because of interaction between the ethanol and solute cluster, the short interactions (CC) were occurred between the monomer molecule that this phenomena affected the birth of different polymorphic forms and created the *form II* with dimeric structure.

Definition of Two Crystalline Packing Polymorphism and Their Relationship to Photoluminescence Behavior Based on Aggregation Induced Enhanced Emission Process (AIEE)

To obtain profound overview into the interesting luminescent behavior of *form I* and *form II* in the aggregate state, the relationship between the packing polymorphism and photophysical results was examined. The packing polymorphism of the two crystal forms depend on molecular conformation which shows large discrepancy between the two polymorphic forms and noncovalent interactions including nonclassical hydrogen bonds, stacking interactions and C···H interactions. The single crystal structure of *form I* contains intra-intermolecular nonclassical hydrogen bonds which are C9—*H*9··· N1 and C12—H12··· N1, respectively and intermolecular strong stacking interactions while *form II* has intra-intermolecular stacking interactions and Cg···Cl1 (Cg3:C11/C16) interactions. In addition *form II* include strong N1···H9 and H25 intermolecular short interactions in which the bond lengths are shorter than vander waals radius between the N and H atoms (2.75) Figure 2.

D-π···A type conjugated molecules usually show unusual fluorescence behavior due to their intramolecular charge transfer (ICT) transitions which contribute to aggregation induced emission in solid phase. In addition, aggregation induced enhanced emission (AIEE) is frequently ascribed to restricted intramolecular rotation (RIR), structural planarity, twisting structure and stacking types (from *H type* to herringbone type). Variation of the solid state luminescence color is less affordable than in solution due to the difficulty in obtaining different stable phases in the aggregated state with varied molecular conformations. This goal can be reached either by obtaining a compound crystallizing in different polymorphs. The molecular packing mode is sensitive o the external conditions such as solvent and temperature, allowing the possibility to form polymorphism which has a significant effect in optoelectronic field. In this study to obtain the

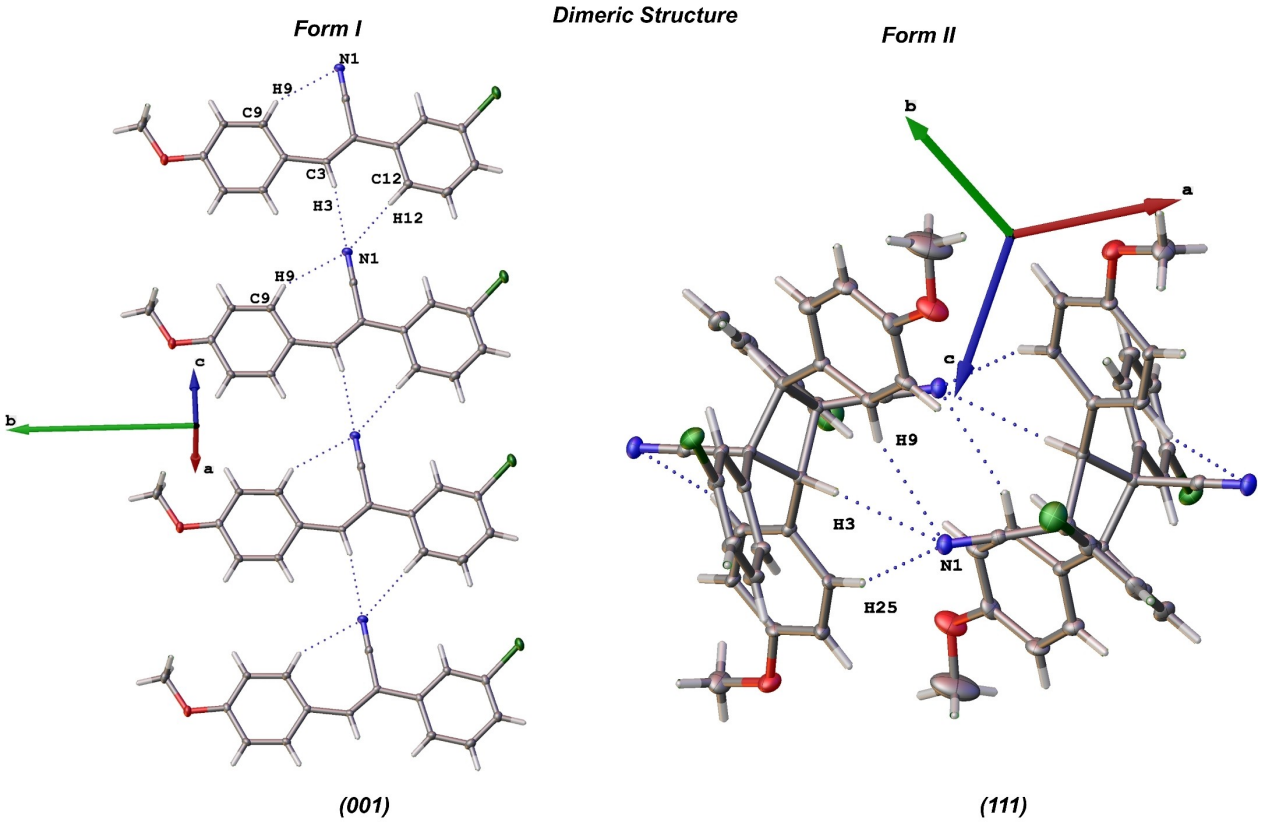


Figure 2. 1D supramolecular dimeric structure of the polymorphic forms with the nonclassical intermolecular hydrogen bonds along the (*001*) plane.

© 2021 Wiley-VCH GmbH

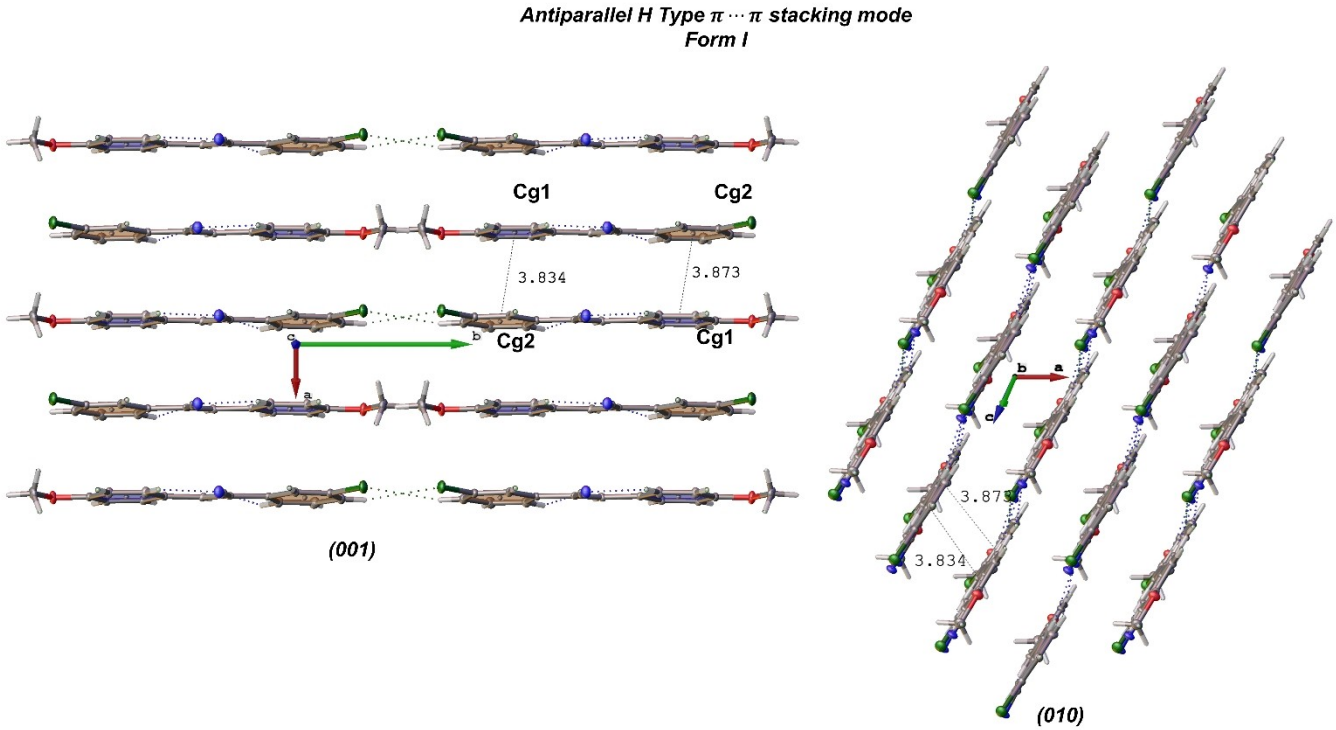


Figure 3. The strong intermolecular anti parallel *H type* stacking interactions of the *form I* with the 3.834 between the stacking rings along the (*001*) and (*010*) planes.

polymorphism dependent aggregation induced emission process, we studied the effects of moelcular conformation on the aggregate packing which strongly affects to fluorescence behavior of the molecule in the solid state.

The intra and intermolecular nonclassical hydrogen bonds in *form I* resulted in restricted intramolecular rotation between the rings that the dimeric structure is created by these interactions whereas the strong short interactions lead to **RIR** proces and form the dimeric structure in the *form II*. Restricted intramolecular rotation (**RIR**) is one of the important concept to determine the aggregation induced emission since the radiationless decay is prevented through the this process.

Another important key for the AIEE process is the packing arrangement of the molecules. In this study, two polymorphic structures of the molecule demonstrated different molecular packings which were created by stacking interactions, nonclassical hydrogen bonds, short interactions and C interactions due to the conformational polymorphism. It is worth mentioning that stacking mode has a decisive effect on the photoluminesance behavior in solid phase. Therefore the *form I* molecule demonstrated 1D supramolecular structure (Cg1···Cg2 with the 3.873 Å perpendicular distance) (Figure 3 and 4, Table 1) created by antiparallel *H* type stacking mode while the *form II* molecule has 1D supramolecular cage and 3D helical supramolecular structure cerated by *J* type stacking interactions (Cg3···Cg2, Cg2···Cg5 and Cg5···Cg5 with the 4.396, 4.193 and 4.682 perpendicular distances, respectively. (Figure 5 and 6, Table 1).[64–70] In addition, Cg···Cl1(Cg3:C11/C16) interactions helps to crystal stabilization of the *form II* molecule and enable contribution to AIEE process through the restricted intramolecular rotation (Figure 7).

When the planarity of π-conjugated materials is increased, the great overlap between π-orbitals of neighbouring molecules occurs that this phenomena results in delocalization of the polarons/excitons and leads to reduction in the energy band gap for charge transport, thereby increasing charge carrier mobilities. Although the *H stacking type* among the all stacking types provide more overlap between the adjacent molecules, the antiparallel *H stacking type* is benefical for the enhancing PL intensity therefore charge carrier and device performance. In particular, benefitting from both the opposite electrostatic potentials on the terminal sides of the molecule, the *form I* crystallized in an antiparallel cofacial stacking mode with tiny displacements and result in increasing photoluminesans intensity in solid phase compared with the that of solution phase (nearly 4 times).

Both forms of the molecule displayed aggregation induced enhanced emission (AIEE) property in the solid phase due to the restricted intramolecular rotation (RIR) and favourable stacking interactions including the antiparallel *H type* and *J type* stacking modes and intramolecular charge transfer (ICT) process. Therefore, we show that polymorhism dependent aggregation induced enhanced emission in solid state for both forms and the effect of the molecular conformation arised from

© 2021 Wiley-VCH GmbH

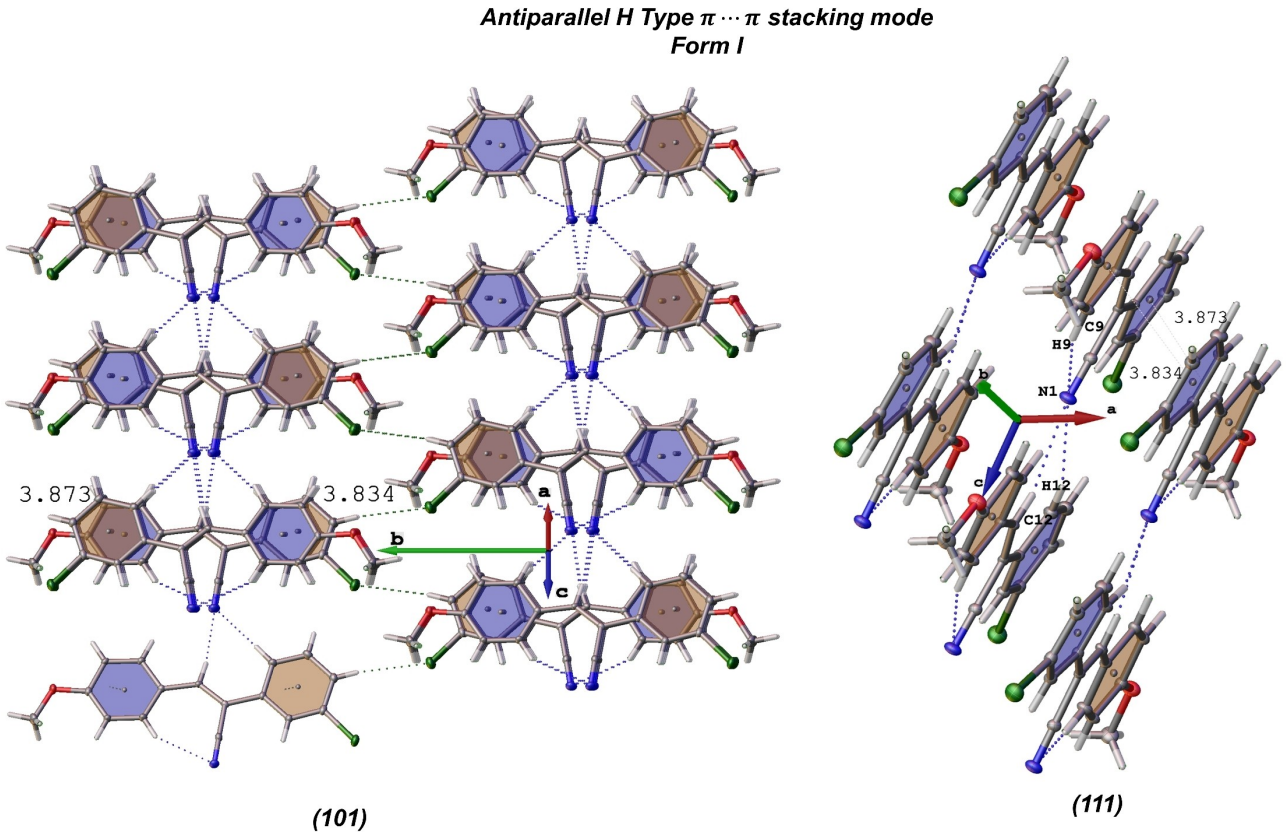


Figure 4. The strong *H type* intermolecular stacking interactions of the *form I* with the intra and intermolecular nonclassical hydrogen bonds along the (*101*) and (*111*) planes.

Table 1. Intermolecular stacking geometries of the polymorphic structures.

Form I			
Stacking parameters	Cg1···Cg2	Cg1···Cg2	
Pitch angle (P:°)	2.4(3)	2.4(3)	
Roll angle (R:°)	24.7	21.1	
Pitch distance(d_P:Å)	0.16	0.16	
Roll distance (d_R:Å)	1.78	1.47	
Slipping angle (β)	26.0	23.3	
Interplanar distance (d)	3.873(4)	3.834(4)	
Symmetry code	−1/2+x,1/2-y,−1/2+z	1/2+x,1/2-y,1/2+z	
Form II			
Stacking parameters	Cg5···Cg2	Cg5···Cg5	Cg3···Cg3
Pitch angle (P:°)	9.5(4)	42.5(4)	42.1
Roll angle (R:°)	34.1(4)	9.1(4)	7.3
Pitch distance(d_P:Å)	0.70(2)	4.29	3.97
Roll distance (d_R:Å)	2.84(2)	0.74	0.56
Slipping angle (β)	27.1	42.5	42.1
Interplanar distance (d)	4.193	4.682	4.396
Symmetry code	x,1-y,1/2+z	2-x,y,3/2-z	1-x,y,1/2-z

polymorphism on the photoluminescence behavior of the polymorphs. When we compare photoluminescence intensity of the *form II* with the *form I*, it is observed that the *form II* demonstrated higher photoluminescence intensity than that of *form* I in solid phase (nearly 2.72 times for *form I* and 35.7 times for *form II*). The enhanced fluorescence intensity in solid phase is strongly related to charge transport rate of the molecules as well as stacking interactions modes. The stacking interactions create charge pathway channels between the neighbouring molecules, which strongly depends on the electronic coupling of the molecules. Electronic coupling closely related to the overlap of HOMO and LUMO between two adjacent molecules.

© 2021 Wiley-VCH GmbH

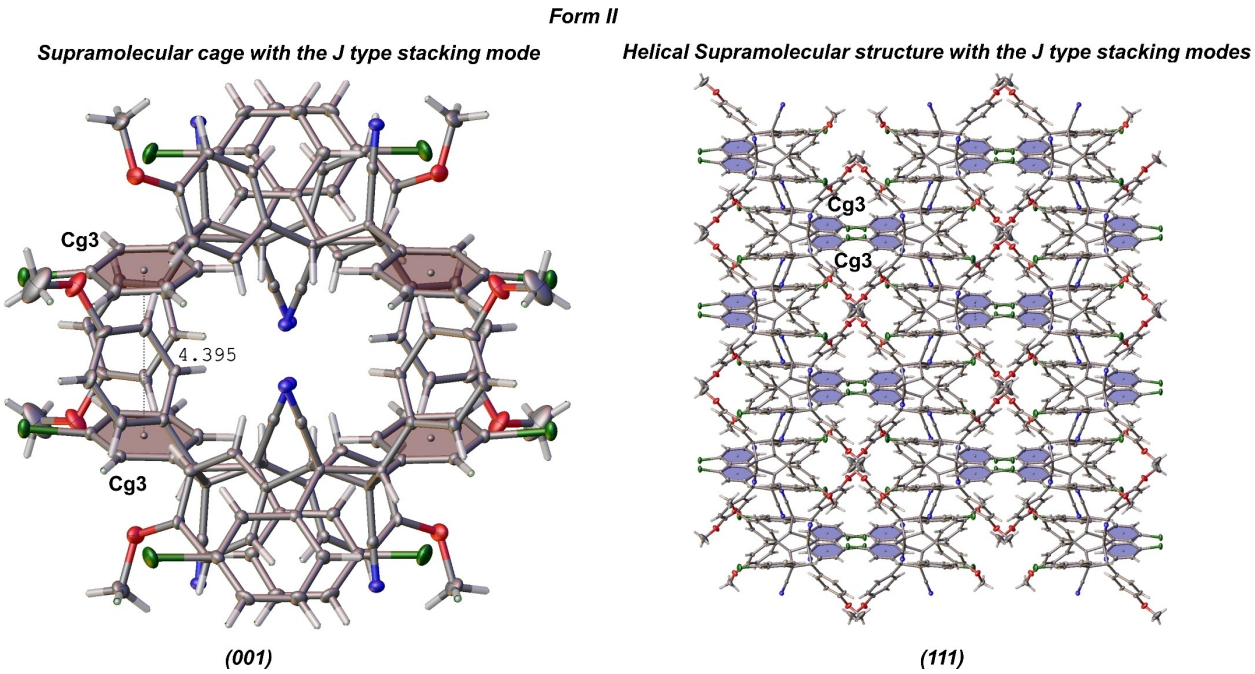


Figure 5. The supramolecular cage and helical formation of *form II* with the *J type* intermolecular stacking interactions having the 4.39 perpendicular distance between the Cg3· · ·Cg3 rings along the (*001*) and (*111*) planes, respectively.

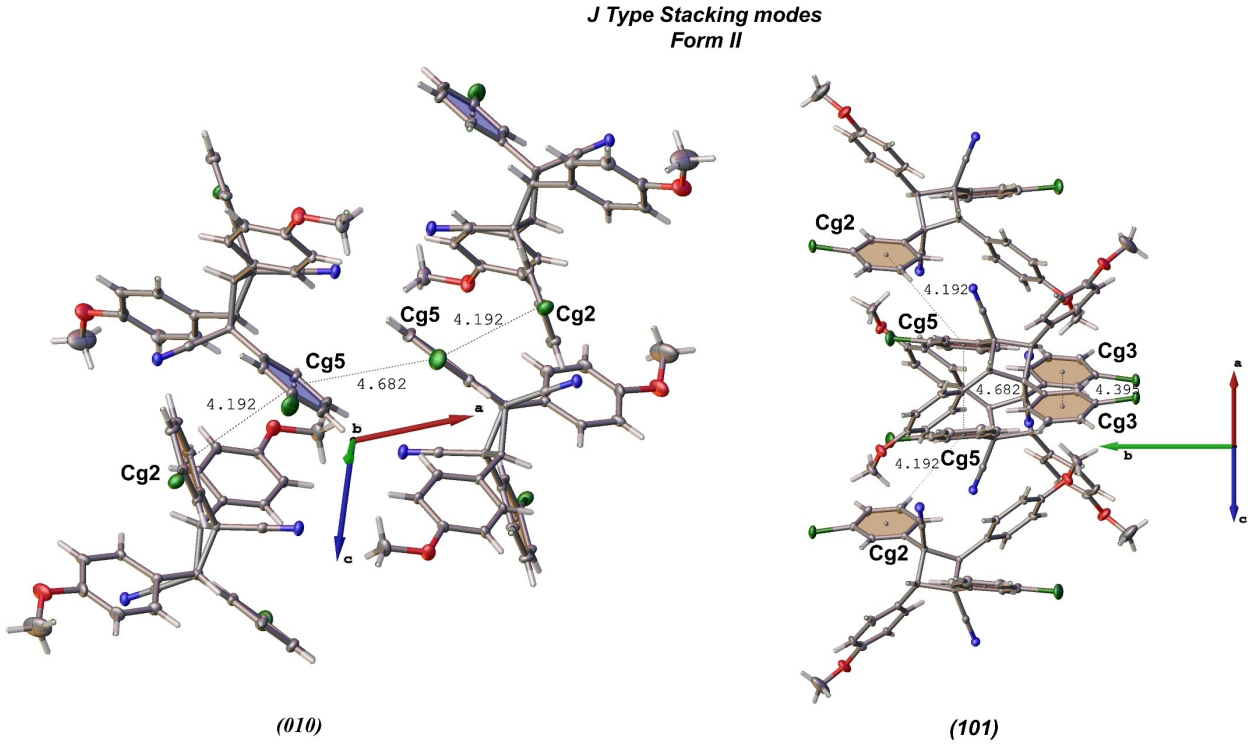


Figure 6. The *J type* stacking modes of the *form II* with the strong intermolecular stacking interactions with the 4. 192 perpendicular distance between the C5 and C2 rings along the (*010*) and (*101*) planes, respectively

In addition, the charge transport rate or luminescence can be affected with other interactions such as, C–H, C-halogen, van-der-Waals forces, e.t.c.[71] In the light of the this concept, the charge pathway channels and electronic coupling were created along the C–Cl direction which result in parallel displaced (J type stacking mode) in the packing arrangement of the *form II*.

© 2021 Wiley-VCH GmbH

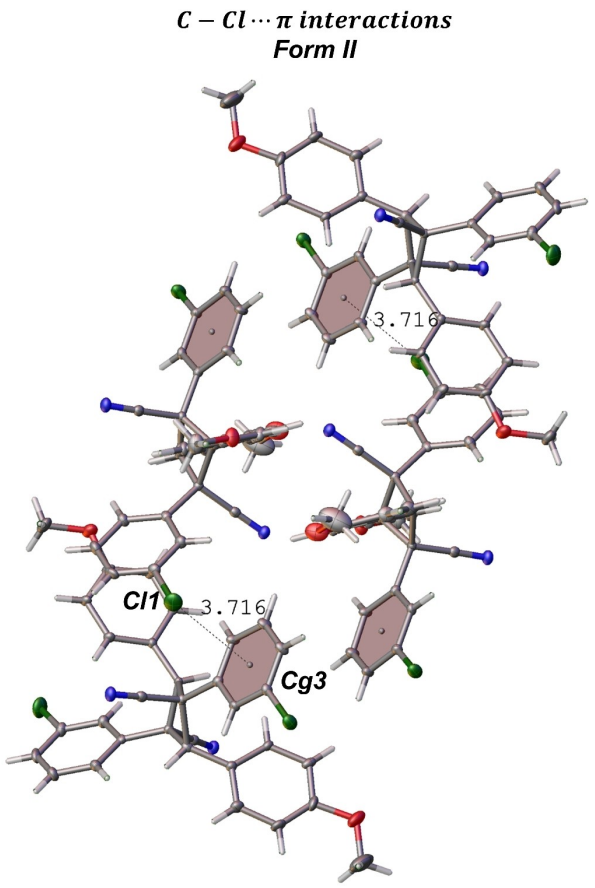


Figure 7. The intermolecular C—*Cl* $\cdots \pi$ interactions of *Form II* (C29)

Although the stacking interaction of the *form II* is weaker than that of *form I*, the strong C–Cl interactions with the short centroid distances contribute to enhanced luminescence in solid phase with the favourable stacking type (J type). As a result, the main reason of fluorescence intensity difference between the two forms is short interactions, twisting structure and J type stacking mode of *form II* which gives high fluorescence emission in solid phase. Therefore, since the phenyl rings of the *form II* have steric hindrance, undesirable face to to face $\pi \cdots \pi$ stacking interactions (parallel *H type* stacking mode) were prevented that this would inevitably have detrimental effect for the fluorescence efficiency. In the *form I*, due to the perfect planarity, strong restricted intramolecular rotation via nonclassical hydrogen bonds and the antiparallel *H type* stacking mode enable to enhanced fluorescence intensity in aggregate phase. As a result, thanks to *J type* and *antiparallel H type* stacking mode which are the favourable stacking types in optoelectronic field with the restricted intramolecular rotation, both forms showed agregation induced enhanced emission in the solid state.

Photophysical Results

The optical characterization of the compounds *form I* and *form II* in solution (2×10^{-5} M) and solid phases were investigated by photoluminescence (PL) and UV-Vis absorption (UV) spectra. The UV-Vis absorption spectra are shown in Figure 8 and the photophysical data are summarized in Table 2.[72] PL properties of *form I* and *form II* under excitation of 349 nm at room temperature were recorded 350–900 nm as depicted in Figure 9.

According to the photoluminescence spectra, *form I* exhibits cyan-blue emission at 468 nm (in solid-state) and 503 nm (in

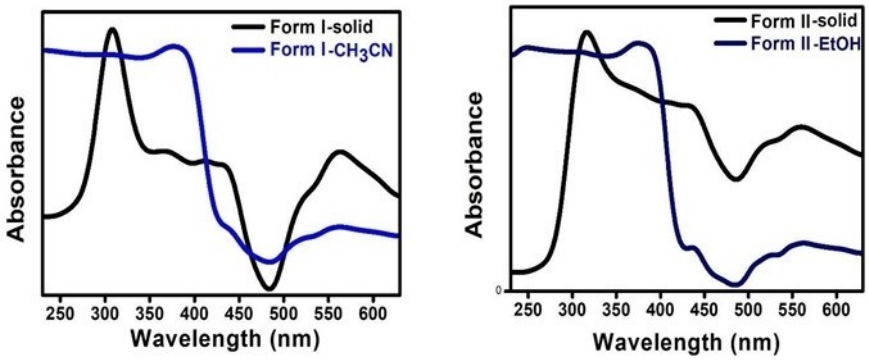


Figure 8. The UV-vis absorption spectra of (a) *form I* in CH_3CN and solid-phase and (b) *form II* in EtOH and solid-phase.

Table 2. The photophysical properties of *form I* and *form II* at different phases.

Ligand	λ_{abs}(nm)[a,c]	λ_{abs}(nm)[b]	λ_{emis}(nm)[a,c]	λ_{emis}(nm)[b]	Stokes Shift[a,c]	Stokes Shift[b]
Form I	378	307	503	468	124	161
Form II	375	314	535	501	158	187

[a]In CH_3CN solution (2×10^{-5} M). [b]In solid-state. [c]In EtOH solution (2×10^{-5} M).

© 2021 Wiley-VCH GmbH

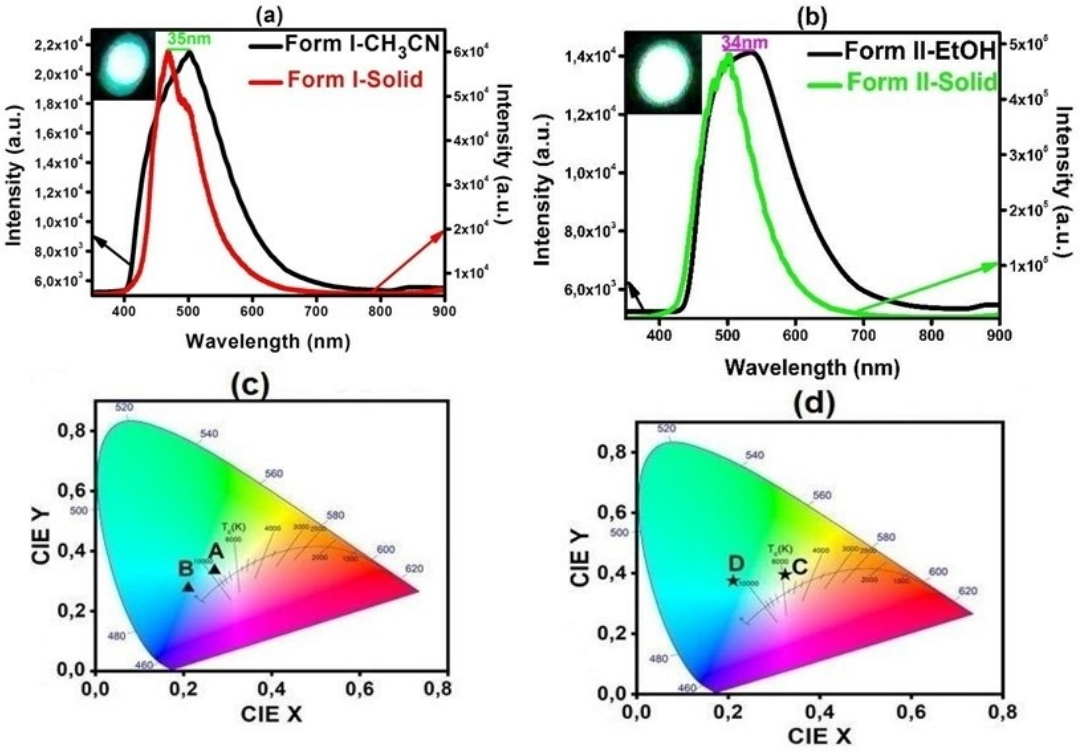


Figure 9. PL spectra for all samples at room temperature (a) *Form I* in CH_3CN and solid-phase and (b) **Form II** in EtOH and solid-phase (inset: The upper-left photo is a photoluminescent image) The emission spectra were excited at 349 nm. Color coordinates in the CIE chromaticity diagrams of (c) *form I* and (d) *form II*.

solution state), while Form II shows green emission at 501 nm (solid-state) and 535 nm (in solution state) (Figure 9a and 9b). Also, the maximum emission wavelength of *form II* shows a significant red shift compared to that of Form I.[73] This red shifted could arise from strong C and stacking interaction in the Form II. Furthermore, photoluminescence emissions at room temperatures suggest that although both forms of the molecule have aggregation induced enhanced emission (AIEE) in solid phase, there is little PL emission gains (about 2.72 times) for form I crystal phase, however, for *form II* crystal phase, large emission enhancement (about 35.7 times) resulted that are compared to their solution phase. This discrepancy can be explanied by the stacking types of the forms since the photoluminecence behavior strongly depends on the molecular arrangements of the both forms. As a result, J type stacking interactions make the molecule higly fluorescent.

The Commission Internationale de l'Eclairage (CIE) color coordinates determined for **A** (*form I* in solid), **B** (Form I in CH_3CN) and **C** (Form II in solid) and **D** (Form II in EtOH) (0.32, 0.39), (0.21, 0.37) and (0.27, 0.33) and (0.21, 0.27) respectively (Figure 9c and 9d). This undoubtedly illustrates that *form I and form II* polymorphs emit almost white light. (0.33, 0.33).[74] Figure 8 illustrates the UV-Vis absorption spectra of *form I* and *form II* in solution (2×10^{-5} M) and solid state. *Form I* and *II* exhibit similar behavior. The solid-state and solution state absorption bands of Form I were observed at around 307 and 378 nm, respectively. As for *form II*, its absorption bands centered at around 314 nm (solid-state) and 375 nm (solution-state). These bands could be attributable to the π- π* transition.[75]

In the background of the above results, we suggest that *form I* represents H-aggregation, while *form II* has J-aggregation which can be accredited to two main factors: (i) It is observed that the emission wavelength of *form II* was significantly red-shifted with 150–180 nm and (ii) *form II* (solid phase) photoluminescence intensity enhances a notable has increased that it is almost near 25 times that of *form I*.

The total integrated intensities as a function of excitation power density are shown in Figure 10 of all solid samples. As seen from Figure 10 total integrated intensity increases with the increase of excitation power density. Further, to understand the nature of the from lower energy peaks to higher energy peaks, we performed excitation power-dependent PL measurements as shown in Figure 10. The main peaks in the higher energy region shift to lower energy with increasing laser power density. At high excitation power density (above the 0.53 Watt/cm^2) is expected to contribute to the red-shifted main peak position.[76]

The transmittance (T) spectra of the *form I* in CH_3CN and solid-phase are shown in Figure 11a. As seen in Figure 11a, the transmittance values of the *form I* in CH_3CN and solid-phase change drastically with changing wavelength. In particular, peak transmittance peaks are observed at wavelengths of about 485 nm. Also, there are significant differences between

© 2021 Wiley-VCH GmbH

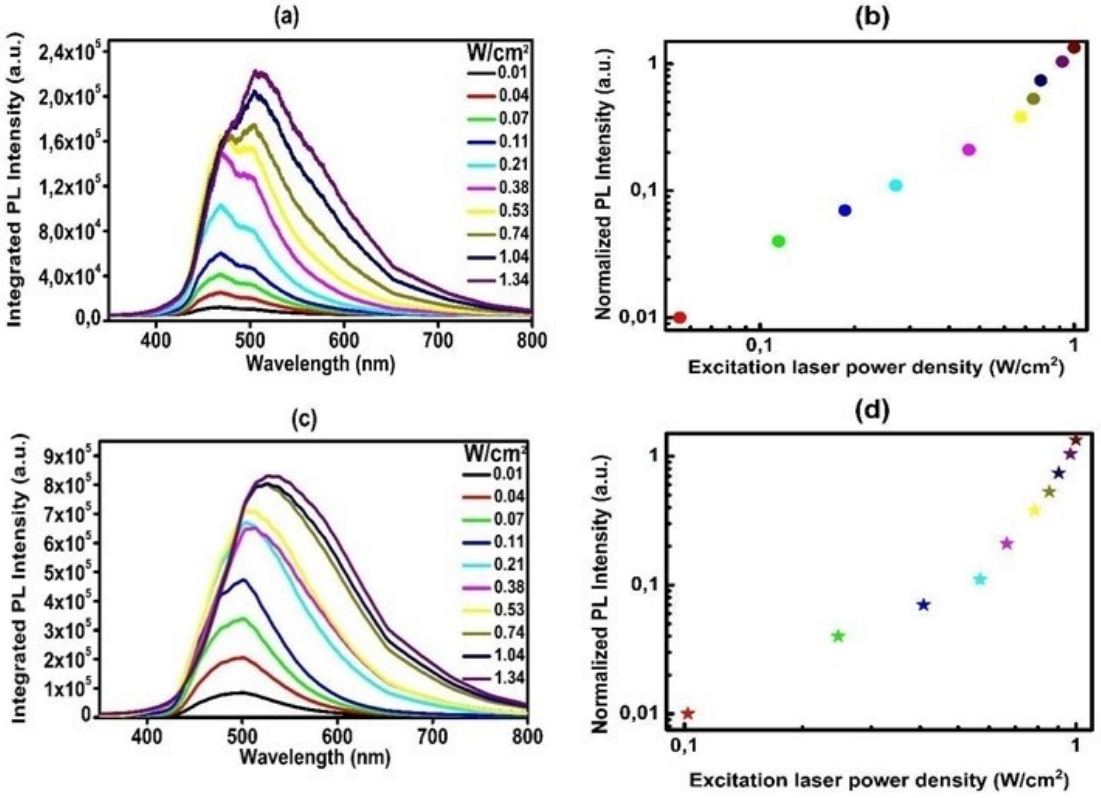


Figure 10. The total integrated intensity versus excitation power density in solid-phase (a) *Form I* and (c) *Form II*. Logarithmic plots of the normalized PL intensity versus excitation-power density (b) *Form I* and (d) *Form II*.

the two curves at low wavelengths. This can be attributed to the dissolution state of the material in the solvent and the element concentration of the solid region interacting with light. The absorption band edge ($E_{Abs\text{-}be}$) values of the *form I* in CH_3CN and solid-phase were obtained from the first derivation ($dT/d\lambda$) vs. wavelength (λ) as seen in Figure 11b. The $E_{Abs\text{-}be}$ values of the *form I* in CH_3CN and solid-phase were found as 2.584 and 2.570 eV, respectively. Although these values are close to each other, they show that the *form I* is promising for optoelectronic applications.

Similarly, the transmittance spectra of the *form II* in EtOH and solid-phase are shown in Figure 11c. As seen in Figure 11c, the curves of the *form II* also differ like the *form I*. Also, the significant differences between solid and solution measurements apply to the *form II*. On the other hand, the absorption band edge values of the *form II* in EtOH and solid-phase were obtained from the $dT/d\lambda$ vs. λ as seen in Figure 11d. The $E_{Abs\text{-}be}$ values of the *form II* in EtOH and solid-phase were found as 2.579 and 2.557 eV, respectively.

Optical band gap (E_g) is an indispensable parameter in the field of optoelectronics. We obtained the optical band gaps of the *form I* and *form II* using Tauc relation.[77] First, we investigated the suitability of the *form I* and *form II* material in optoelectronic applications. From the curves drawn, it was seen that the optical transition type of both materials was directly allowed band pass. This shows that the *form I* and *form II* are very suitable for use in optoelectronic fields. For this, we first plotted the $(\alpha h\nu)^2$ (α is absorption coefficient and $h\nu$ is photon energy) plots vs E of the Form I in CH_3CN and solid-phase and of the Form II in EtOH and solid-phase as seen in Figure 12 (a,b), respectively. The direct optical band gaps of the *form I* in CH_3CN and solid-phase were found as 2.685 and 2.554 eV, respectively (see Figure 10a). On the other hand, the direct optical band gaps of the *form II* in EtOH and solid-phase were found as 2.580 and 2.534 eV, respectively (see Figure 12b). These results show that the optical band gaps of the *form I* and *form II* are in the band gap of semiconductors.

Another critical parameter for the optoelectronic field is the refractive index (n). The refractive indices of the *form I* and *form II* material were calculated from various relations such as Moss, Ravindra, Herve-Vandamme, Reddy and Kumar-Singh.[78] The refractive indices obtained are as shown in Figure 13 (a, b). The refractive indices of *form I* and *form II* material are of different values for different relations. The average refractive index of both materials is around 2.5. This value is at a very good level for optoelectonic applications.

Theoretical Results

To obtain more information about the molecular frontier orbitals energy levels, energy band gap ($E_{band\ gap}$) and intra-molecular charge transfer properties of the polymorphic

© 2021 Wiley-VCH GmbH

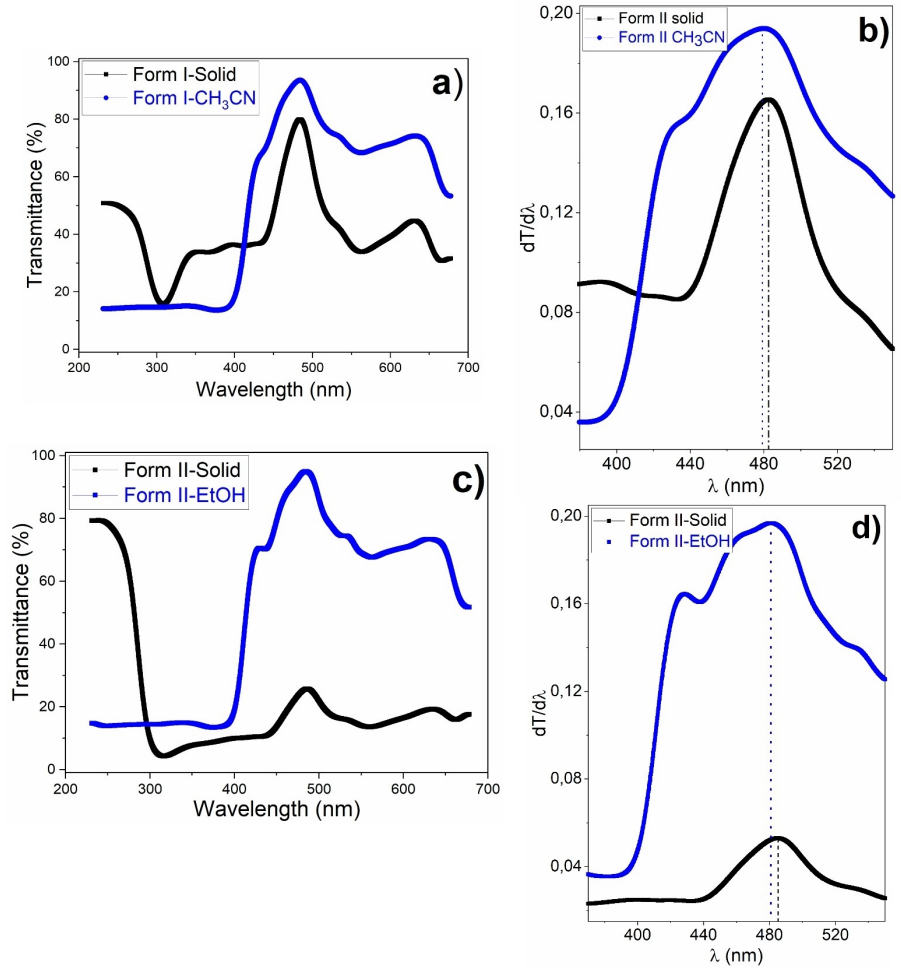


Figure 11. The **a**) transmittance (T) spectra, **b**) dT/dλ plots vs. wavelength (λ) of the *form I* in CH_3CN and solid-phase and **c**) T spectra **d**) dT/dλ plots vs. λ of the *form II* in EtOH and solid-phase.

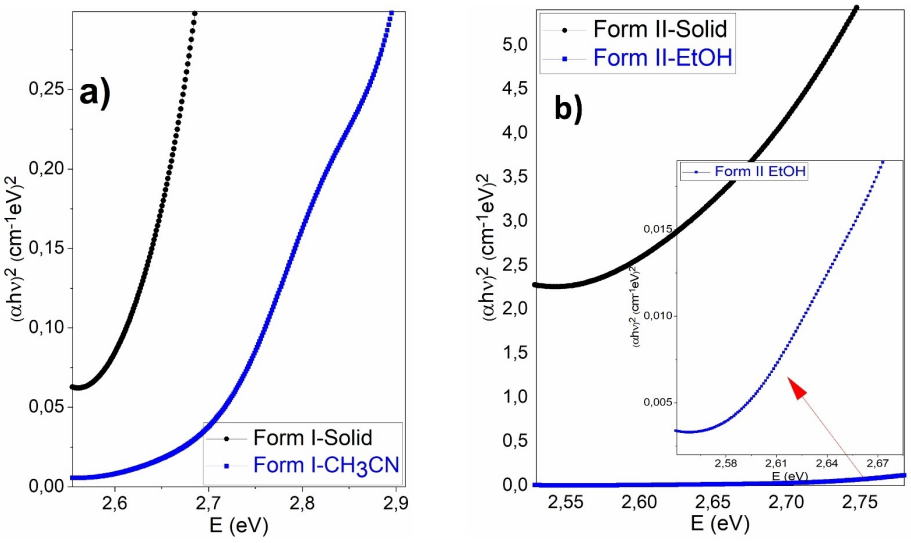


Figure 12. The $(\alpha h\nu)^2$ plot vs. photon energy (E) of the **a**) *Form I* in CH_3CN and solid-phase and **b**) *Form II* in EtOH and solid-phase.

© 2021 Wiley-VCH GmbH

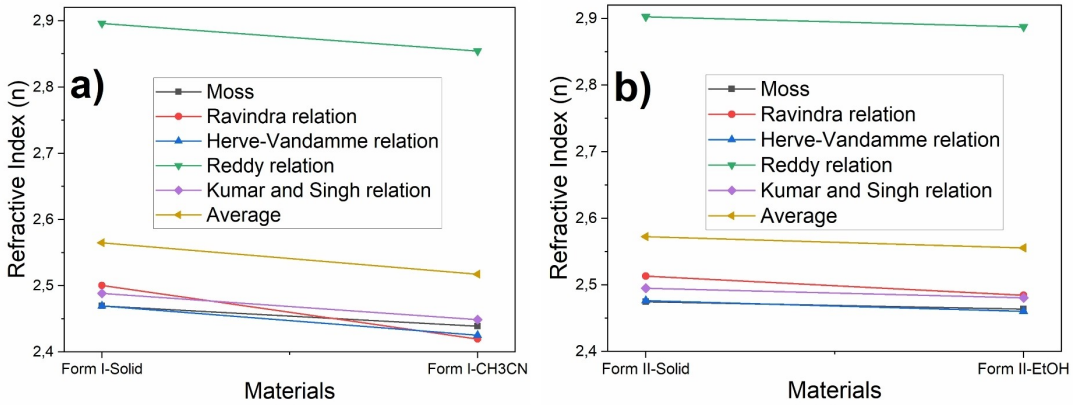


Figure 13. The refractive indices of the **a)** *Form I* in CH_3CN and solid-phase and **b**) *Form II* in EtOH and solid-phase for various relations.

structures, Density Functional Theory (DFT) and Time Dependent Density Functional Theory (TDDFT) were applied in the gas phase with complete geometry optimization at the ground-state structures through CAM-B3LYP/6-31G(d,p) level. The most favourable optimized structures of the molecules which are good aggrement with single crystal XRD view are given in the Figure S4.

Thanks to frontier molecular orbitals, the chemical reactivity and kinetic stability of the molecules could be understant in detail. Chemical interactions between the adjacent molecules in the aggregate state can be determined through frontier orbitals (FMOs), as well. Most chemical reactions occur by giving or receiving electrons, thus HOMOs and LUMOs have direct effect on molecular structures. It is worth mentioning that intramolecular charge transfer (ICT) which is responsible for aggregation induced enhanced emission (AIEE) mechanism in solid phase can be improved by attaching electron donors and acceptors groups to the compound. In the D-π-A molecules, the polarization which is related to molecular dipole moment of the molecule occurs in the π-electrons of the molecule skeleton since the electron acceptor group withdraws electronic charge from the donor through the conjugated structure. Interaction between donor acceptor groups called intramolecular charge transfer (ICT) forms low energy molecular orbital. The selected frontier orbtal distributions of the polymorphic forms are depicted in Figure 14 and 15. HOMO,

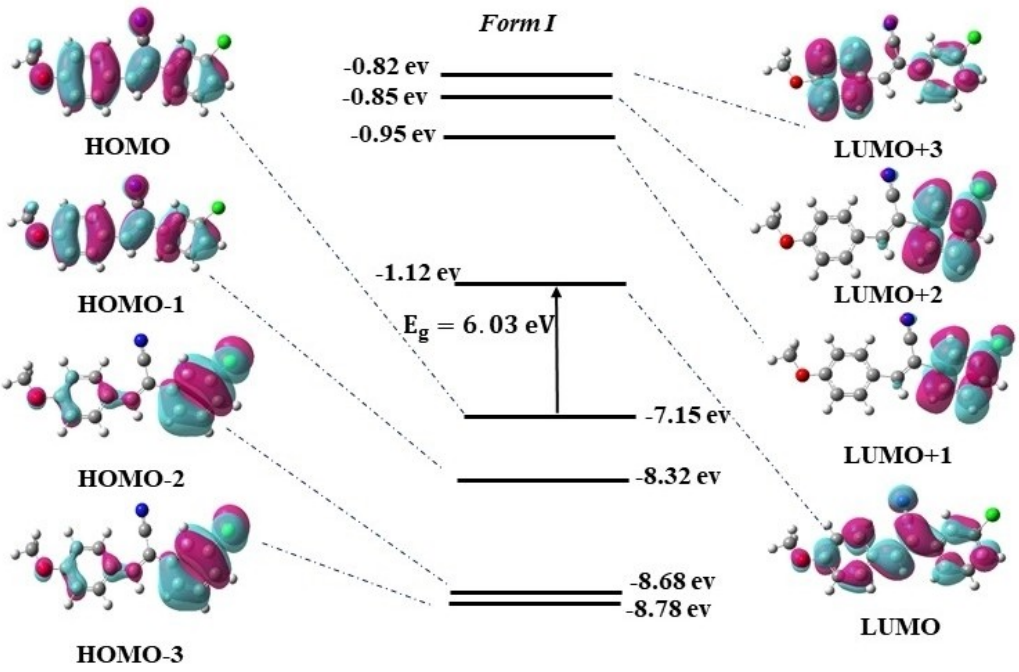


Figure 14. Energy levels for selected occupied and unoccupied molecular orbitals of *form I* obtained by DFT calculations using CAM-B3LYP-631G (d,p) basis set..

© 2021 Wiley-VCH GmbH

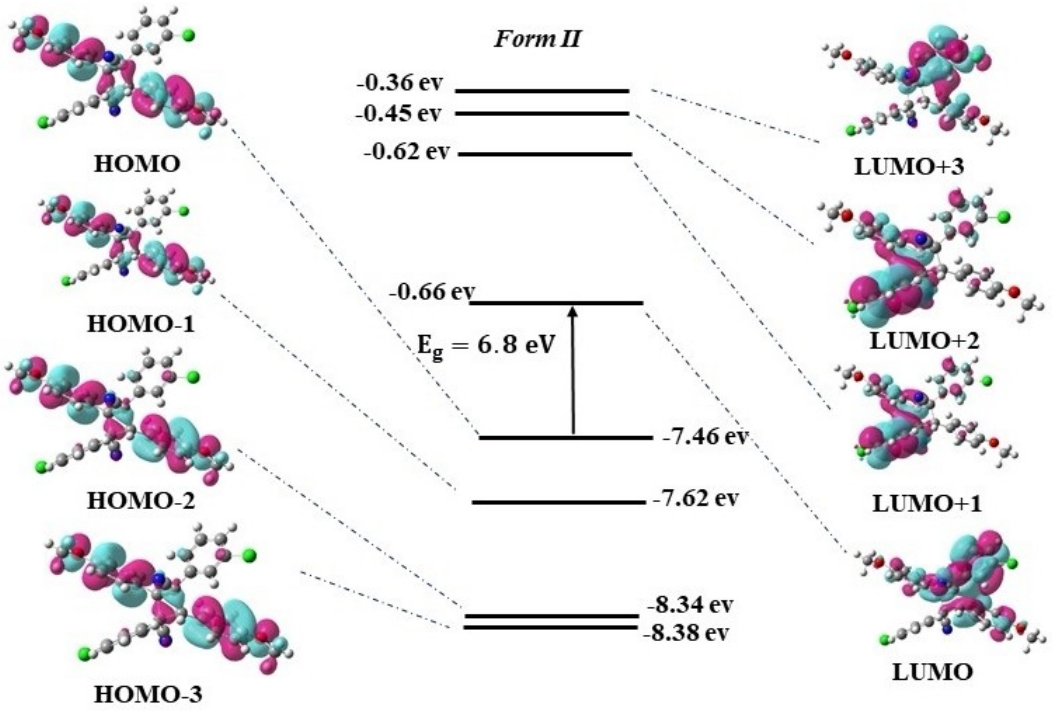


Figure 15. Energy levels for selected occupied and unoccupied molecular orbitals of *form II* obtained by DFT calculations using CAM-B3LYP-631G (d,p) basis set..

LUMO, HOMO + 1, HOMO + 2, HOMO + 3, LUMO-1, LUMO-2 and LUMO-3 molecular orbitals were influenced by structural polymorphism. Therefore, the discrepancy between the frontier orbitals between of polymorpic forms arises from the different molecular and single crystal structure.

HOMO and HOMO-1 orbital of *form I* were delocalized over the donor and acceptor moieties (OCH3, CN) of the molecule while they were distributed over the methoxyphenyl rings of the *form II* as the electron-donating character of substituents increases. For the *form I,* LUMO orbital was localized over the donor and acceptor sides of the molecule whereas LUMO + 1 orbital distribution decreased in the chlorophenyl ring as as the electron-donating propensity increases. For the *form II*, LUMO and LUMO + 1 orbitals mainly located electron acceptor groups. Both forms displayed a major charge-transfer transition from a methoxyphenyl delocalized HOMO and HOMO-1 to a chlorphenyl and cyano moities delocalized LUMO and LUMO + 1, respectively, due to efficient HOMO/LUMO overlap and the strong electron-withdrawing ability of the CN unit. Therefore, in the both forms, intramolecular charge transport which plays important role in the aggregation induced enhanced emission (AIEE) mechanism is mainly controlled by the electronic transitions from HOMOs to LUMOs. Since π stacking interactions of the *form I* and *form II* obtained from single crystal x-ray crystallography data include efficient HOMOs- LUMOs overlap which increases electron attraction process with the *H* and *J* π stacking modes, respectively, the solid phase fluorescence intensity of the both forms is considerable high compared to the that of solution phase.

Conclusion

In summary, two polymorphs of a (E)-2-(3-chlorophenyl)-3-(4-methoxyphenyl)acrylonitrile molecule has been investigated to analyze the photophysical behavior in solid and solution state through single crystal x-ray crystallography, photophysical studies and theoretical calculations. Single Crystal X-ray Crystallography investigations revealed that the molecular arrangement and molecular conformation in the polymorphs are substantially different. Therefore, solid state fluorescence behavior of the polymorphs was observed to be dependent on the morphology forms. Intermolecular interactions including stacking interactions, nonclassical hydrogen bonding and C interactions in the crystal phase of the polymorphs cause to different emission behavior in solid phase with one emitting in the cyan blue region while the other emits in the green. In addition, both form of the molecule displayed aggregation induced enhanced emission (AIEE) process in the solid phase due to the restricted intramolecular rotation (RIR) and favourable stacking interactions and intramolecular charge transfer (ICT) process. However, *form II* demonstrated more fluorescence emission increase than *form I* in solid phase compared to that of solution phase (nearly 2.72 times for *form I* and 35.7 times for *form II*). The main reason of fluorescence intensity difference between the two forms is short interactions, twisting structure and *J* type stacking mode of *form II* which gives high fluorescence emission in solid phase since the charge pathway channels and electronic coupling were created along the C–Cl direction which result in parallel displaced (J type stacking mode) in the packing arrangement of the *form II.* Therefore,

© 2021 Wiley-VCH GmbH

since the phenyl rings of the *form II* have steric hindrance, undesirable face to to face $\pi\cdots\pi$ stacking interactions (parallel *H type* stacking mode) were prevented that this would inevitably have detrimental effect for the fluorescence efficiency. In the *form I*, due to the perfect planarity, strong restricted intramolecular rotation via nonclassical intramolecular hydrogen bonds, the antiparallel *H type* stacking mode enables to enhanced fluorescence intensity in aggregate phase. As a result, *J type* and antiparallel *H type* stacking mode with the restricted intramolecular rotation make the crystals higly emissive in solid phase. Thus, our study verifies the importance of the molecular conformation, molecular arrrangement created by the stacking interactions in aggregated state, stacking interactions type and takes a great attention for the development of new acrylonitrile derivative through the polymorphism.

Deposition Number(s) 2081145 (for form **1**), 2081146 (for form **2**) contain the supplementary crystallographic data for this paper. These data are provided free of charge by the joint Cambridge Crystallographic Data Centre and Fachinformationszentrum Karlsruhe Access Structures service www.ccdc.cam.ac.uk/structures.

Supporting Information Summary

Synthesis and characterization details of *form I* and *form II* are given in supporting information.

Acknowledgements

This work was supported by the Akdeniz University and Dokuz Eylul University. Many thanks for financial support of The Scientific and Technological Research Council of Turkey (TUBITAK, KBAG-119Z608) and Akdeniz University Scientific Research Projects Unit (AU-BAP, Big Issue FBA-2020-5403). The authors acknowledge the Dokuz Eylul University for the use of the Agilent Xcalibur Eosdiffractometer (purchased under University Research grant no. 2010.KB.FEN.13) and Gaussian Software Programme.

Conflict of Interest

The authors declare no conflict of interest.

Keywords: Acrylonitrile Derivatives · Conformational Polymorphism · Crystal Engineering · DFT · Fluorescence

[1] Y. Geng, A. Tang, K. Tajima, Q. Zeng, E. Zhou, *J. Mater. Chem. A* **2019**, *7*, 64.
[2] M. Bendikov, F. Wudl, D. F. Perepichka, *Chem. Rev.* **2004**, *104*, 4891–4945.
[3] H. Sirringhaus, *Adv. Mater.* **2014**, *26*, 1319.
[4] P. E. Hartnett, A. Timalsina, H. S. S. R. Matte, N. Zhou, X. Guo, W. Zhao, A. Facchetti, R. P. H. Chang, M. C. Hersam, M. R. Wasielewski, T. J. Marks, *J. Am. Chem. Soc.* **2014**, *136*, 16345.
[5] S. Varghese, S. Das, *J. Phys. Chem. Lett.* **2011**, *2*, 863.
[6] H. Li, X. Zhang, Z. Chi, B. Xu, W. Zhou, S. Liu, Y. Zhang, J. Xu, *Org. Lett.* **2011**, *13*, 556.
[7] M. Mas-Torrent, C. Rovira, *Chem. Rev.* **2011**, *111*, 4833.
[8] A. Facchetti, *Chem. Mater.* **2011**, *23*, 733.
[9] M. Brinkmann, G. Gadret, M. Muccini, C. Taliani, N. Masciocchi, A. Sironi, *J. Am. Chem. Soc.* **2000**, *122*, 5147.
[10] E. Cho, C. Risko, D. Kim, R. Gysel, N. Cates Miller, D. W. Breiby, M. D. McGehee, M. F. Toney, R. J. Kline, J. L. Bredas, *J. Am. Chem. Soc.* **2012**, *134*, 6177.
[11] N. S. Saleesh Kumar, S. Varghese, C. H. Suresh, N. P. Rath, S. Das, *J. Phys. Chem. C* **2009**, *113*, 11927.
[12] T. Nicolini, A. Famulari, T. Gatti, J. Martí-Rujas, F. Villafiorita-Monteleone, E. V. Canesi, F. Meinardi, C. Botta, E. Parisini, S. V. Meille, C. Bertarelli, *J. Phys. Chem. Lett.* **2014**, *5*, 2171.
[13] M. Sen Yuan, D. E. Wang, P. Xue, W. Wang, J. C. Wang, Q. Tu, Z. Liu, Y. Liu, Y. Zhang, J. Wang, *Chem. Mater.* **2014**, *26*, 2467.
[14] F. Bu, R. Duan, Y. Xie, Y. Yi, Q. Peng, R. Hu, A. Qin, Z. Zhao, B. Z. Tang, *Angew. Chem. Int. Ed.* **2015**, *54*, 14492.
[15] E. D. Głowacki, M. Irimia-Vladu, S. Bauer, N. S. Sariciftci, *J. Mater. Chem. B* **2013**, *1*, 3742.
[16] Y. Chen, J. W. Y. Lam, R. T. K. Kwok, B. Liu, B. Z. Tang, *Mater. Horiz.* **2019**, *6*, 428.
[17] B. Dong, M. Wang, C. Xu, Q. Feng, Y. Wang, *Cryst. Growth Des.* **2012**, *12*, 5986.
[18] D. Braga, F. Grepioni, L. Maini, M. Polito, *Structure and Bonding* **2009**, *132*, 25.
[19] I. Barsky, J. Bernstein, *CrystEngComm* **2008**, *10*, 669.
[20] H. Zhang, Z. Zhang, K. Ye, J. Zhang, Y. Wang, *Adv. Mater.* **2006**, *18*, 2369.
[21] A. M. Master, M. E. Rodriguez, M. E. Kenney, N. L. Oleinick, A. Sen Gupta, *J. Pharm. Sci.* **2010**, *99*, 2386.
[22] O. D. Jurchescu, D. A. Mourey, S. Subramanian, S. R. Parkin, B. M. Vogel, J. E. Anthony, T. N. Jackson, D. J. Gundlach, *Phys. Rev. B: Condens. Matter Mater. Phys.* **2009**, *80*, 21.
[23] K. Kersten, R. Kaur, A. Matzger, *IUCrJ* **2018**, *5*, 124.
[24] B. Huang, W.-C. Chen, Z. Li, J. Zhang, W. Zhao, Y. Feng, B. Z. Tang, C.-S. Lee, *Angew. Chem.* **2018**, *130*, 12653.
[25] S. Long, P. Zhou, S. Parkin, T. Li, *CrystEngComm* **2015**, *17*, 2389.
[26] S. Long, S. Parkin, M. Siegler, C. P. Brock, A. Gammers, T. Li, *Cryst. Growth Des.* **2008**, *8*, 3137.
[27] B. Moulton, M. J. Zaworotko, *Chem. Rev.* **2001**, *101*, 1629.
[28] K. Wang, H. Zhang, S. Chen, G. Yang, J. Zhang, W. Tian, Z. Su, Y. Wang, *Adv. Mater.* **2014**, *26*, 6168.
[29] B. Fraboni, A. Fraleoni-Morgera, Y. Geerts, A. Morpurgo, V. Podzorov, *Adv. Funct. Mater.* **2016**, *26*, 2229.
[30] S. Yoon, J. W. Chung, J. Gierschner, K. S. Kim, M. Choi, D. Kim, S. Y. Park, M. C-ix, A. V. Toma, *J. Am. Chem. Soc.* **2010**, *132*, 13675–13683.
[31] J. Yang, Z. Ren, B. Chen, M. Fang, Z. Zhao, B. Z. Tang, Q. Peng, Z. Li, *J. Mater. Chem. C* **2017**, *5*, 9242.
[32] D. Alducin, B. D. Myers, X. Liu, B. L. Fisher, *Nanomaterials* **2015**, *350*, 1513–1516.
[33] C. Sutton, C. Risko, J. L. Brédas, *Chem. Mater.* **2016**, *28*, 1, 3–16.
[34] Q. Li, Z. Li, *Acc. Chem. Res.* **2020**, *53*, 962.
[35] A. Nangia, *Acc. Chem. Res.* **2008**, *41*, 595.
[36] R. Montis, M. B. Hursthouse, H. C. S. Chan, J. Kendrick, F. J. J. Leusen, *CrystEngComm* **2012**, *14*, 1672.
[37] H. Chung, Y. Diao, *J. Mater. Chem. C* **2016**, *4*, 3915.
[38] F. Chen, Y. Wang, W. Zhang, T. Tian, B. Bai, H. Wang, F. Q. Bai, M. Li, *Cryst. Growth Des.* **2019**, *19*, 6100.
[39] Y. F. Chang, Z. Y. Lu, L. J. An, J. P. Zhang, *J. Phys. Chem. C* **2012**, *116*, 1195.
[40] Z. Xie, B. Yang, L. Liu, Y. Ma, *Journal of Molecular and Engineering Materials* **2013**, *01*, 1340002.
[41] H. Jiating, X. Bin, C. Feipeng, X. Haijian, L. Kunpeng, Y. Ling, T. Wenjing, *J. Phys. Chem. C* **2009**, *113*, 9892.
[42] L. Yu, *Acc. Chem. Res.* **2010**, *43*, 1257.
[43] Q. L. Xu, X. Liang, L. Jiang, Y. Zhao, Y. X. Zheng, *Dalton Trans.* **2016**, *45*, 7366.
[44] R. Pfattner, M. Mas-Torrent, I. Bilotti, A. Brillante, S. Milita, F. Liscio, F. Biscarini, T. Marszalek, J. Ulanski, A. Nosal, M. Gazicki-Lipman, M. Leufgen, G. Schmidt, W. M. Laurens, V. Laukhin, J. Veciana, C. Rovira, *Adv. Mater.* **2010**, *22*, 4198.
[45] X. Cheng, F. Li, S. Han, Y. Zhang, C. Jiao, J. Wei, K. Ye, Y. Wang, H. Zhang, *Sci. Rep.* **2015**, *5*, 1.
[46] S. K. Seth, A. Bauzá, A. Frontera, *New J. Chem.* **2018**, *42*, 12134.

© 2021 Wiley-VCH GmbH

[47] S. K. Seth, P. Manna, N. J. Singh, M. Mitra, A. D. Jana, A. Das, S. R. Choudhury, T. Kar, S. Mukhopadhyay, K. S. Kim, *CrystEngComm* **2013**, *15*, 1285.
[48] F. Liang, J. Chen, Y. Cheng, L. Wang, D Ma, X. Jing, F. Wang, *J. Mater. Chem.* **2003**, *13*, 1392–1399.
[49] C. A. Hunter, *Angew. Chem. Int. Ed. Engl.* **1993**, *32*, 1584.
[50] N. S. S. Kumar, M. D. Gujrati, J. N. Wilson, *Chem. Commun.* **2010**, *46*, 5464.
[51] M. D. Curtis, J. Cao, J. W. Kampf, *J. Am. Chem. Soc.* **2004**, *126*, 4318.
[52] J. H. Dou, Y. Q. Zheng, Z. F. Yao, Z. A. Yu, T. Lei, X. Shen, X. Y. Luo, J. Sun, S. D. Zhang, Y. F. Ding, G. Han, Y. Yi, J. Y. Wang, J. Pei, *J. Am. Chem. Soc.* **2015**, *137*, 15947.
[53] F. C. Spano, *Acc. Chem. Res.* **2010**, *43*, 429.
[54] J. Chen, B. Z. Tang, *Aggregation-Induced Emission: Fundamentals and Applications* **2013**, *1–2*, 307.
[55] C. Wang, Z. Li, *Mater. Chem. Front.* **2017**, *1*, 2174.
[56] L. Le Bras, K. Chaitou, S. Aloïse, C. Adamo, A. Perrier, *Phys. Chem. Chem. Phys.* **2019**, *21*, 46.
[57] W. Z. Yuan, P. Lu, S. Chen, J. W. Y. Lam, Z. Wang, Y. Liu, H. S. Kwok, M. Yuguang, B. Z. Tang, *Adv. Mater.* **2010**, *22*, 2159.
[58] Y. Hong, J. W. Y. Lam, B. Z. Tang, *Chem. Commun.* **2009**, *29*, 4332–4353.
[59] J. Luo, Z. Xie, Z. Xie, J. W. Y. Lam, L. Cheng, H. Chen, C. Qiu, H. S. Kwok, X. Zhan, Y. Liu, D. Zhu, B. Z. Tang, *Chem. Commun.* **2001**, *18*, 1740.
[60] J. Chen, C. C. W. Law, J. W. Y. Lam, Y. Dong, S. M. F. Lo, I. D. Williams, D. Zhu, B. Z. Tang, *Chem. Mater.* **2003**, *15*, 1535.
[61] E. M. El-Menyawy, A. A. Elagamey, S. R. Elgogary, R. A. N. Abu El-Enein, *Spectrochim. Acta Part A* **2013**, *108*, 75.
[62] L. Cao, M. Dong, A. Zhang, Y. Liu, W. Yang, Z. Su, X. Chen, *Polym. Eng. Sci.* **2013**, *53*, 2674.
[63] M. Hranjec, G. Pavlović, M. Marjanović, M. Kralj, G. Karminski-Zamola, *ChemMedChem.* **2010**, *45*, 2405.
[64] D. Piovesan, G. Minervini, S. C. E. Tosatto, *Nucleic Acids Res.* **2016**, *44*, W367.
[65] R. Thomas, S. Varghese, G. U. Kulkarni, *J. Mater. Chem. C* **2009**, *19*, 4401.
[66] C. R. Martinez, B. L. Iverson, *Chem. Sci.* **2012**, *3*, 2191.
[67] J. Hermann, D. Alfè, A. Tkatchenko, *Nat. Commun.* **2017**, 14052, 1–8.
[68] Z. F. Yao, J. Y. Wang, J. Pei, *Cryst. Growth Des.* **2018**, *18*, 1, 7–15.
[69] R. Zhao, R. Q. Zhang, *Phys. Chem. Chem. Phys.* **2016**, *18*, 25452.
[70] A. Banerjee, A. Saha, B. K. Saha, *Cryst. Growth Des.* **2019**, *19*, 2245.
[71] M. Liu, Y. Wei, Q. Ou, P. Yu, G. Wang, Y. Duan, H. Geng, Q. Peng, Z. Shuai, Y. Liao, *J. Phys. Chem. Lett.* **2021**, *12*, 938.
[72] X. Zhang, J. Ye, L. Xu, L. Yang, D. Deng, G. Ning, *J. Lumin.* **2013**, *139*, 28.
[73] X. Zhang, J. Wang, Y. Liu, Y. Hao, F. Yu, D. Li, X. Huang, L. Yu, T. Wang, H. Hao, *Catal. Sci. Technol.* **2021**, *11*, 943–955.
[74] A. R. Mallia, R. Sethy, V. Bhat, M. Hariharan, *J. Mater. Chem. C* **2016**, *4*, 2931.
[75] H. Wang, F. Chen, X. Jia, H. Liu, X. Ran, M. K. Ravva, F. Q. Bai, S. Qu, M. Li, H. X. Zhang, J. L. Brédas, *J. Mater. Chem. C* **2015**, *3*, 11681.
[76] H. R. Byun, D. Y. Park, H. M. Oh, G. Namkoong, M. S. Jeong, *ACS Photonics* **2017**, *4*, 2813.
[77] B. Gündüz, *Opt. Mater.* **2013**, *36*, 425.
[78] S. K. Tripathy, *Opt. Mater.* **2015**, *46*, 240.

Submitted: June 7, 2021
Accepted: October 21, 2021

© 2021 Wiley-VCH GmbH